NCEP DYNAMICAL SEASONAL FORECAST SYSTEM 2000

BY MASAO KANAMITSU, ARUN KUMAR, HANN-MING HENRY JUANG, JAE-KYUNG SCHEMM, WANQUI WANG, FANGLIN YANG, SONG-YOU HONG, PEITAO PENG, WILBER CHEN, SHRINIVAS MOORTHI, AND MING JI

NCEP's newly developed second-generation operational seasonal forecast system aims at a seamless suite of forecasts and provides much more comprehensive datasets for users.

In April 2000, a new dynamical seasonal prediction system was introduced at the National Centers for Environmental Prediction (NCEP; the acronyms used in this paper are summarized in the appendix). The transition to the new system was hastened by a computer fire in September 1999 and subsequent changeover from a Cray C90 to an IBM-SP computer system. This article will be a reference for people who are using the NCEP numerical seasonal forecast products.

The first-generation dynamical seasonal prediction model was based on the notion that the seasonal predictability in the Northern Hemisphere extratropics mainly stems from equatorial tropical Pacific sea surface temperature anomalies (SSTA). This predictability motivated the NCEP Coupled Modeling Project to couple the atmospheric model with a Pacific basin ocean model (Ji et al. 1995). A major effort was made to build an ocean data assimilation system and a coupled prediction system to produce skillful SSTA forecasts over the tropical Pacific and to improve the physical parameterizations of the atmospheric model to better simulate the middle-latitude atmospheric response to anomalous tropical SST forcing. This approach led to successful wintertime seasonal predictions (Ji et al. 1995; Kumar et al. 1996; Behringer et al. 1998; Ji et al. 1998).

The second-generation dynamical seasonal prediction is designed 1) to further improve the coupled modeling system to refine wintertime prediction, and 2) to take advantage of additional sources of predictability during other seasons. The latter requires incorporating new physical processes. In particular, in recent years the effect of soil moisture shows promise of enhancing summertime predictability (e.g., Koster et al. 2000). Forcing by snow and sea ice may also enhance predictability. Atmospheric initial conditions may also help increase prediction skill. Incorporation of these processes in a dynamical prediction system requires taking care with the initialization procedure.

The dynamical seasonal prediction is still a basic research problem, because our understanding of the

AFFILIATIONS: KANAMITSU—Climate Research Division, Scripps Institution of Oceanography, University of California, San Diego, La Jolla, California; KUMAR, SCHEMM, PENG, AND CHEN—NOAA/NCEP/Climate Prediction Center, Camp Springs, Maryland; JUANG, WANG, YANG, AND MOORTHI—NOAA/NCEP/Environmental Modeling Center, Camp Springs, Maryland, HONG—Department of Atmospheric Sciences, Yonsei University, Seoul, Korea; JI—NOAA/Office of Global Programs, Silver Spring, Maryland
CORRESPONDING AUTHOR: Dr. Masao Kanamitsu, Scripps Institution of Oceanography, 9500 Gilman Drive, Dept. 0224, La Jolla, CA 92093-0224
E-mail: kana@ucsd.edu

In final form 4 April 2002

atmosphere's response to external forcing remains insufficient. Increased understanding usually requires additional idealized experiments. However, operational prediction emphasizes practical aspects of the seasonal forecast and places less emphasis on idealized experiments. Additional coordination between operational and research efforts is absolutely necessary to improve the dynamical seasonal prediction (Roads et al. 2001).

There are at least four major requirements for a successful dynamical seasonal prediction system:

1) accurate and efficient models of atmosphere, ocean, land, and sea ice that are coupled in a physically consistent manner;
2) initial conditions for the atmosphere, ocean, land, and sea ice;
3) an ensemble prediction methodology; and
4) a strategy for systematic error correction.

The first two components are most basic to successful seasonal prediction and are closely tied to each other through data assimilation of a land–atmosphere–ocean system. The model must also run efficiently on a given computer resource and preferably also run on a variety of computers, since dynamical seasonal prediction requires many lengthy integrations. Furthermore, portability of the model codes to different computer platforms eases technology transfer between research and operations. We will describe the new NCEP seasonal prediction system along the line of the requirements stated earlier.

The seasonal forecast system at NCEP adopts a "two tiered" approach. First, SST anomalies over the tropical Pacific are predicted using a coupled ocean–atmosphere model. This tier-one forecast for SST is run weekly using the ocean initial conditions produced from the ocean data assimilation system. A total of four runs are made each week using different atmospheric initial conditions (but the same ocean initial conditions), in order to account for some uncertainties due to "weather" noise in the atmosphere. The SST anomalies are obtained by removing the coupled model climatology estimated from hindcasts over the 1982–98 period. Over a period of 1 month, the weekly SST forecasts aggregate to a 16-member ensemble from which the ensemble mean of the SST forecasts is derived. An example of an ensemble SST forecast and the corresponding observation is shown in Fig. 1.

The second tier of the seasonal forecast system consists of ensemble seasonal forecasts using the atmospheric forecast model alone. The ensemble mean SST forecast obtained from tier one of the forecast system is used as a lower boundary condition to force the seasonal atmospheric model in making the ensemble seasonal forecasts. Since the coupled model forecasts are for the equatorial Pacific region only, we combine the observed SST anomalies outside the equatorial Pacific domain with the forecast SST anomalies to form global SST anomaly fields at the initiation of the tier-two forecasts. The observed SST anomalies outside the equatorial Pacific are damped with an *e*-folding timescale of 3 months for the tropical region (other than the Pacific) and an *e*-folding timescale of 1 month for the extratropics region during the forecast integration. The observed SST anomalies used for this purpose are from the NCEP weekly SST analysis (Reynolds and Smith 1994). The tier-two forecast model predicts both soil wetness and soil temperature throughout the integration period.

The sea ice model is not yet incorporated into the current system. The current plan is to collaborate with GFDL to use their existing sea ice model.

Atmospheric model. The basic dynamical framework of the model is based on the spectral method as described in Kanamitsu (1989). The reduced grid of Williamson and Rosinski (2000) was recently adopted to save

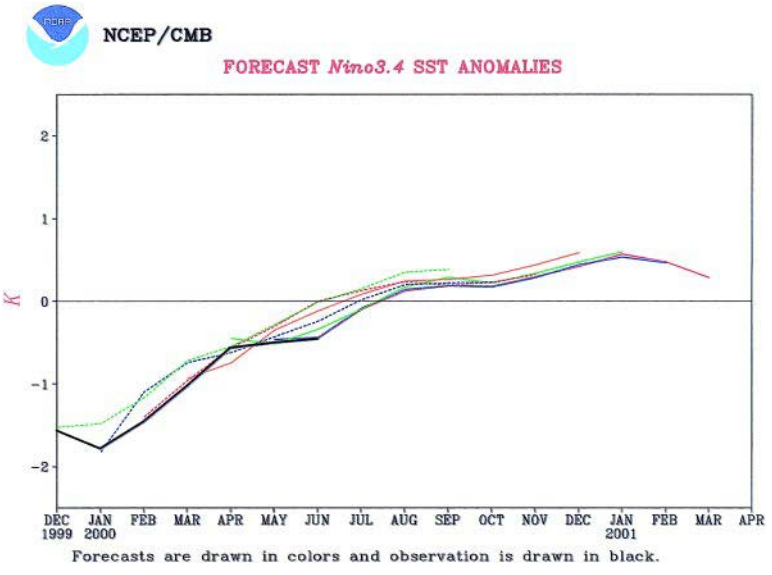

Fig. 1. An example of ensemble SST anomaly forecast over the Niño-3.4 area. Observation is shown as the black line.

computer time without significantly sacrificing accuracy. The reduced grid technique defines the number of zonal waves that can be reduced from the full resolution at given latitude by specifying the desired accuracy to the polynomial multiplication in the Legendre transform calculations. The use of single-digit accuracy saved the computer resources by about 30% at T62 resolution without excessively degrading the long integration in higher latitudes (where the number of grid points is reduced).

The model resolution during April 2000 to March 2001 was unreduced T42 (about 300 km) resolution with 28 layers in the vertical. The horizontal resolution was increased to a T62 reduced grid version (about 200-km resolution) with the same number of vertical layers in April 2001.

The physical processes in the model originated from the NCEP–DOE reanalysis (hereafter referred to as Reanalysis-2) version of the NCEP Medium-Range Forecast (MRF) model (Kanamitsu et al. 2001; manuscript submitted to *Bull. Amer. Meteor. Soc.*). In Table 1, a detailed comparison of model physics is made between the old and new models and the operational MRF. Major improvements over the first version are the use of a more physically based Arakawa–Schubert-type convective parameterization, a multilayer soil model with more complex surface layer physics, and refined planetary boundary layer physics. The physics of the model was modified further from the Reanalysis-2 version based on the result from a series of ENSO response simulation experiments described below.

When the first version of the seasonal prediction model was adapted from the operational MRF model in early 1990, the response of the tropical convection to SSTA, key to successful seasonal prediction, was

Table 1. Comparison of the model physics between three models. SFM is the new version of the seasonal forecast model, B9X is the old version, and MRF is the current operational medium-range prediction model.

	SFM	B9X	MRF
Resolution	T42L28/T62rL28	T42L18	T170L42
Physics			
Convection	RAS (Moorthi and Suarez 1992)	Kuo (Kuo 1965)	SAS (Pan and Wu 1995)
SW radiation	Chou (1992)	Lacis and Hansen (1974)	Chou (1992)
LW radiation	Chou and Suarez (1994)	Fels and Schwarzkopf (1975)	Fels and Schwarzkopf (1975)
Clouds	Slingo (1987)	Slingo (1987)	Function of predicted liquid water
PBL	Nonlocal (Hong and Pan 1996)	Local (Tiedtke 1983)	Nonlocal (Hong and Pan 1996)
Gravity wave drag	Alpert et al. (1988)	Alpert et al. (1988)	Kim and Arakawa (1995)
Land processes	OSU two-layer soil (Pan and Mahrt 1987)	Bucket (Miyakoda and Sirutis 1986)	OSU two-layer soil (Pan and Mahrt 1987)
Orography	Smoothed mean	Smoothed mean	Mean
Ozone	Climatology	Climatology	Predicted
Coding			
Portability	Yes	No	No
MPP	2D decomposition	No	1D decomposition

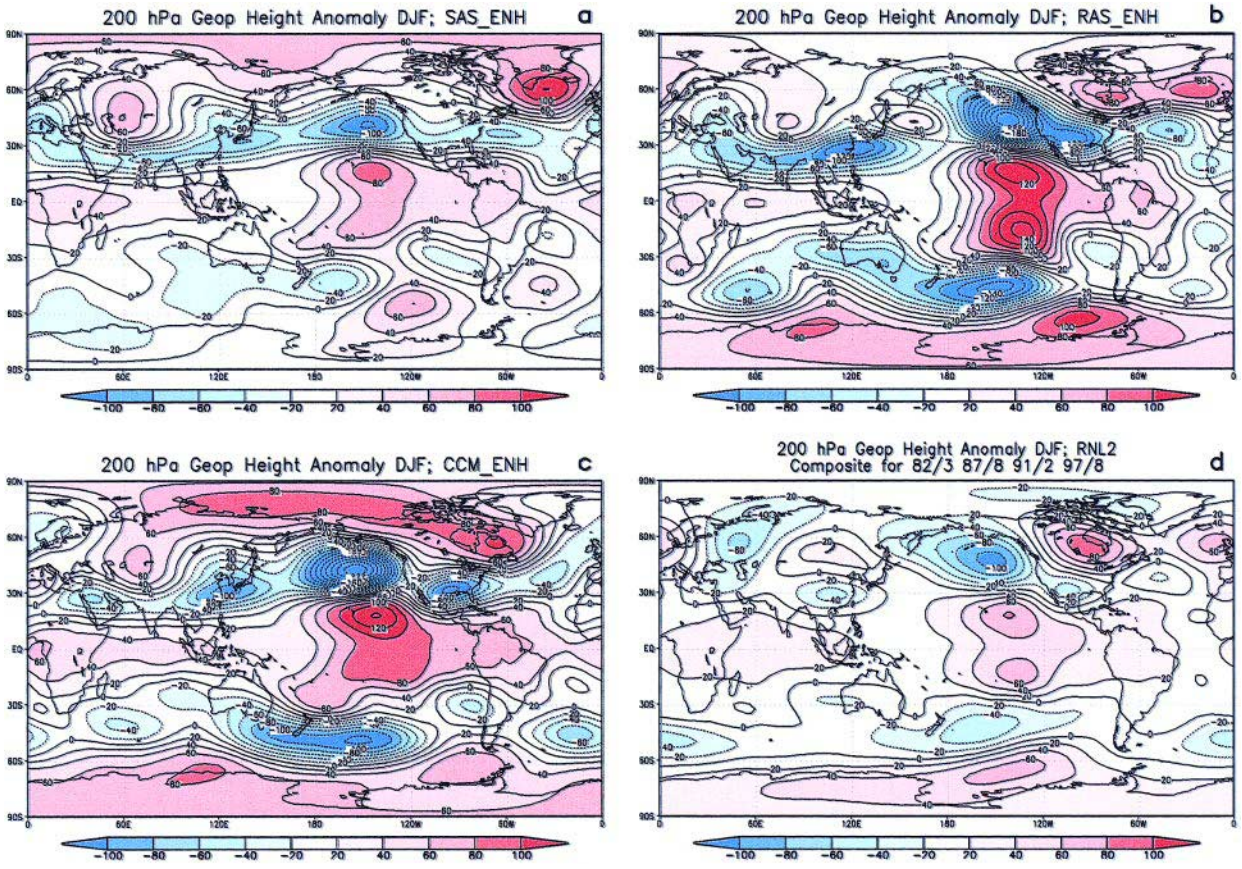

Fig. 2. 200-hPa height anomaly (m) from the idealized ENSO experiment: (a) simplified Arakawa–Schubert scheme, (b) relaxed Arakawa–Schubert scheme, (c) CCM3 Zhang and McFarlane scheme, and (d) observed composite of warm ENSO anomaly (DJF of 1982/83, 1987/88, 1991/92, and 1997/98).

found to be poor in long-term integrations. Kumar et al. (1996) made considerable effort to correct this problem and several modifications were applied to the Kuo convective parameterization scheme to produce a more realistic model response to the equatorial Pacific SSTA. One correction was the application of an SST threshold that triggered convection (Kumar et al. 1996).

Sometime around 1995, the simplified Arakawa–Schubert (SAS) convection scheme (Pan and Wu 1995) replaced the Kuo scheme in the operational MRF and it was used in the NCEP–NCAR Reanalysis (hereafter referred to as reanalysis-1) because it improved prediction of tropical and extratropical precipitation in the short- and medium-range forecasts (Kalnay et al. 1996). We designed an idealized experiment to examine the capability of the SAS convection scheme in long-term integrations. In the experiment, a large-amplitude canonical warm ENSO SSTA of up to 4 K was placed at the western equatorial Pacific. The full annual cycle of SST was obtained by adding the (time invariant) anomaly to the climatological seasonal cycle. Two 10-yr atmospheric integrations were made, one using the anomalous SST and the other with the climatological (background) SST. The difference between these two experiments was considered to be the model response to the SSTA forcing and it was compared to the composite of warm ENSO events from observations. This experiment was designed to test the ability of the model to simulate the most distinct large-scale atmospheric response to El Niño forcing. Therefore, we focused on the conspicuous large-scale patterns of tropical precipitation anomaly, and the intensity and phase of the Pacific–North American (PNA) pattern in the upper atmosphere during the winter season.

The experiments revealed that the SAS scheme has a poor PNA response, particularly over the northern United States and Canada (Fig. 2a). The corresponding tropical precipitation anomaly appears as the zonal band as seen in Fig. 3a, indicating the tropical–extratropical forcing is more zonally symmetric. In addition, the dry anomaly over Indonesia is weak compared to the composite (Fig. 3d), making the

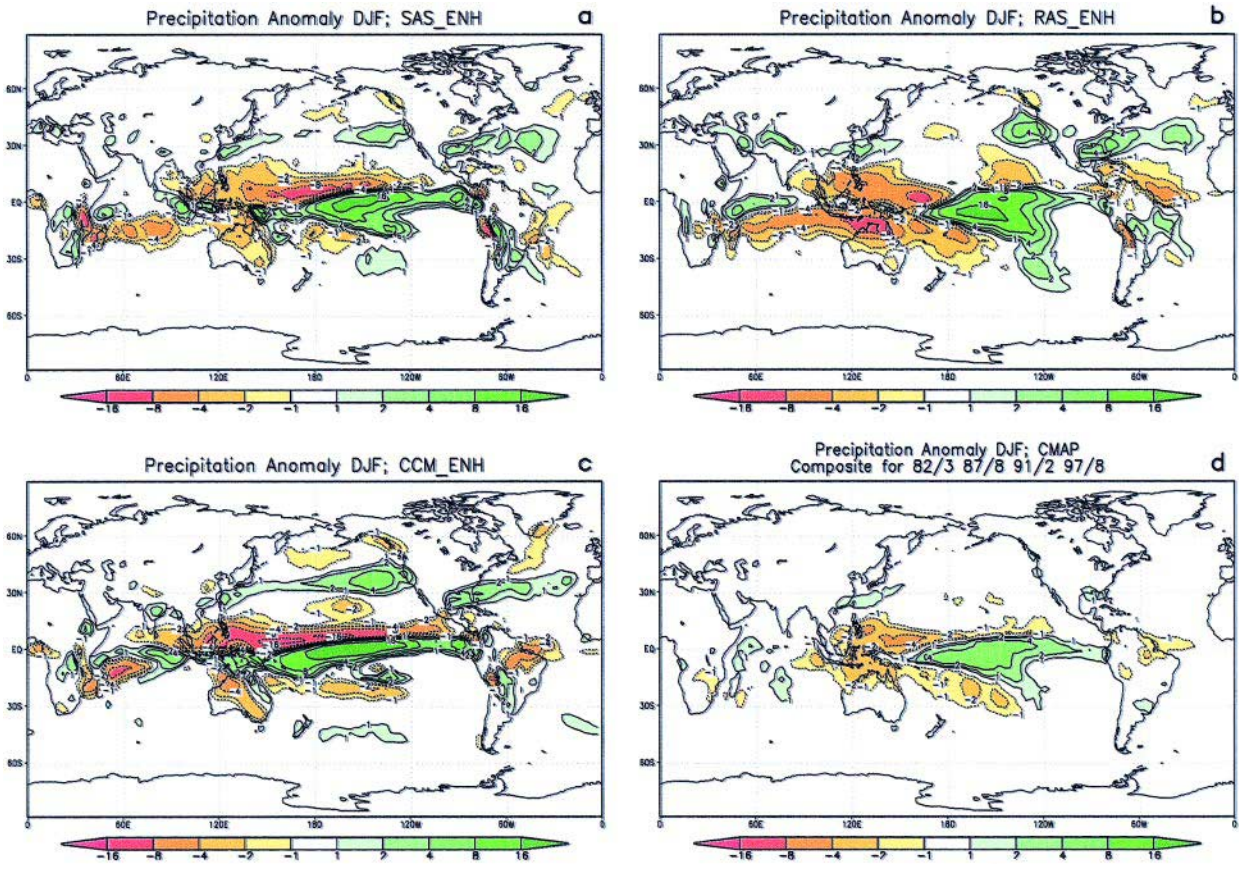

Fig. 3. Same as in Fig. 1 but for precipitation (mm day^{-1}).

forcing zonal over the equatorial zone. This forcing pattern may be related to the poor PNA response of the SAS scheme. We next tested the relaxed Arakawa–Schubert (RAS) convective parameterization scheme (Moorthi and Suarez 1992), which produces reasonable responses in other models (e.g., see Shukla et al. 2000). As shown in Fig. 2b, the RAS scheme significantly improved the PNA response. Zonally asymmetric forcing seems to produce a more realistic wave train.

The main differences between the SAS and RAS are the clouds and the treatment of downdrafts. The SAS allows only one type of cloud, while RAS allows clouds with different tops. The SAS considers saturated downdrafts based on empirical formulation, while RAS (as implemented) does not incorporate any downdraft mechanisms. These differences resulted in different vertical heating and moistening profiles and changed the tropical precipitation. Recently, downdraft mechanisms were introduced in the RAS scheme (Moorthi and Suarez 1999). A preliminary simulation with the new RAS suggested that the lack of downdrafts in RAS may not have been a serious shortcoming.

The same idealized ENSO experiment was performed with the convection scheme (Zhang and McFarlane 1995) used in NCAR Community Climate Model version 3 (CCM3) and the results are shown in Figs. 2c and 3c. With this scheme, the PNA response is excellent while the precipitation anomaly is more zonal (similar to that of SAS). The main difference in the precipitation anomaly of the CCM3 run from that of SAS is in the magnitude of the dry anomaly over Indonesia, which is as large as that of the RAS. These experiments suggest that the heating anomaly over Indonesia may be crucial to the positive height anomaly over the United States.

The PNA response is not the only factor that determines the performance of the model. Two other key factors are noted here; one is the systematic error of the model, and the other is the intraseasonal oscillation. In the current version of the seasonal prediction system, we focused on the systematic error, and left the intraseasonal oscillation for future improvement. The systematic error of the prediction is customarily corrected after the fact, as will be discussed later, but the dynamical effect of the systematic error during the model integration could be one

of the reasons for poor model performance (Kumar et al. 1996).

The Reanalysis-2 model suffers from a warm bias, especially in the polar regions and over continents, which was inherent in the MRF model. An effort was made to reduce these errors in the climate simulations by performing detailed surface energy budget comparisons with the Reanalysis-2. The analysis showed that the downward longwave radiation at the surface was overestimated by several tens of watts per meter squared over the Northern Hemisphere continents. This overestimate was traced to a deficiency in the formulation of clouds. The empirical returning of the clouds dramatically reduced the warm bias (Fig. 4). We also implemented M.-D. Chou's longwave radiation scheme (Chou and Lee 1996) and the original Slingo cloud scheme (Slingo 1987), since the combination of these two also reduced the warm bias. The improvement was considered to be due to 1) the difference in the handling of cloudiness between the MRF (Fels and Schwarzkopf 1975; Schwarzkopf and Fels 1985, 1991) and Chou and 2) the treatment of abnormal water vapor absorption. For the treatment of clouds, the Fels–Schwarzkopf radiation scheme uses maximum cloud overlap and the Chou scheme uses a combination of maximum and random overlap. The use of maximum-random overlap effectively decreased the cloudiness in the Chou scheme, thus leading to the reduction of warm bias (Y.-T. Hou 2001, personal communication). The handling of the abnormal water vapor absorption also explains some of the warm bias in the Fels and Schwarzkopf scheme (F. Yang 2001, personal communication). More study is needed to identify the real cause of the differences.

Another crucial factor in the warm bias was related to the specification of orography. In medium-range predictions, it is well known that enhanced orography increases forecast skill (Jarraud et al. 1988). The enhancement is particularly important for lower-resolution models (ranging from T40-T106) during winter. The idealized warm ENSO experiments described earlier were again performed to test the impact of orography on seasonal integrations. The difference in the PNA response was relatively minor, with a slight westward phase shift in the PNA pattern with an enhancement of orography. The greatest impact of the orography was found in the zonal mean error during the summer time. It was apparent that the enhanced orography acted as an elevated heat source and resulted in a warm bias. The degradation of the summer forecast by the enhanced orography for T40 and T62 resolution is also noted by Jarraud et al. (1988), but not the bias problem.

Further testing of the orography was performed with different smoothing and enhancement combinations, and it was determined that the smoothed mean orography was the best choice for reducing the warm bias without greatly influencing the PNA response. These orography experiments imply that the changes made to improve the medium-range prediction may not necessarily improve the prediction at seasonal timescales. The strong nonlinearity in the long-term integration makes it very difficult to apply the experience in medium-range prediction to longer-range integrations.

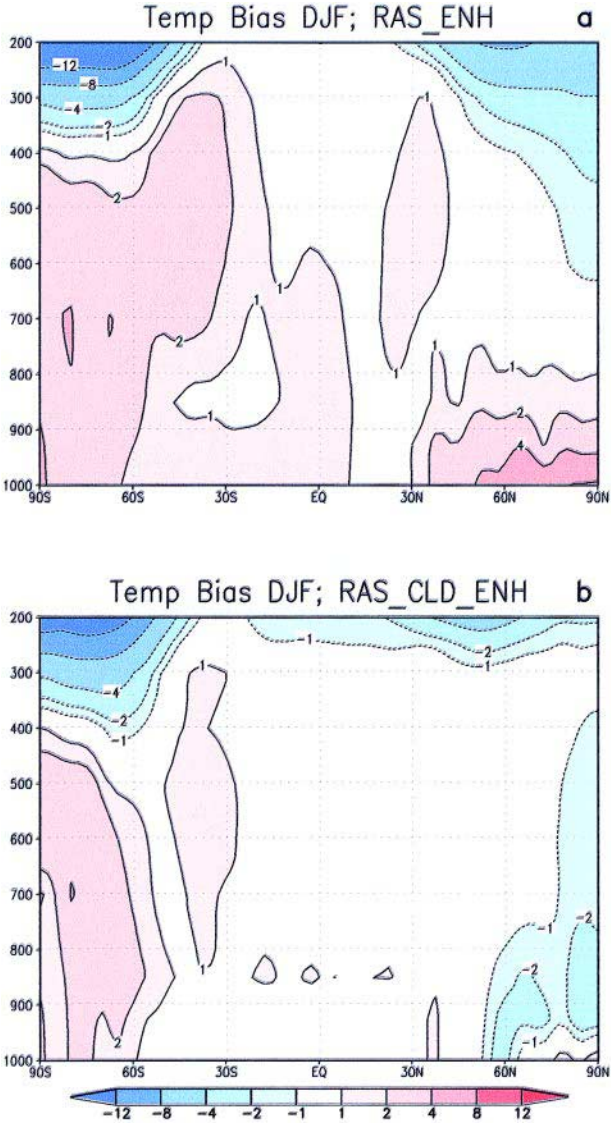

Fig. 4. DJF mean zonally averaged temperature difference (K) between model simulation and Reanalysis-2: (a) control integration with RAS convective parameterization and enhanced orography, and (b) integration with modification in the cloudiness parameterization.

Land model. The land model used in the new system is based on the Oregon State University land model (Pan and Mahrt 1987). Recent changes to the original scheme are found in Chen et al. (1996). The model has two soil layers and predicts soil temperature and water content as well as canopy water content. The vegetation type and cover and soil type are taken from the Simple Biosphere model climatology (Dorman and Sellers 1989). These parameters are a function of space and season. Simple snow physics is also included. The old version used a bucket model (Miyakoda and Sirutis 1986), which had a tendency to generate extreme of soil wetness states. The importance of the complexity in the land model is discussed by Garrat (1993).

The land model is currently coded as a part of the atmospheric model, thus taking full advantage of the model portability to multiple platforms. However, the

MODEL COMPUTER CODE

The computer code of the Reanalysis-2 model was extensively modified to make the model run on multiple platforms with single and/or multiple shared memory machines. The code was improved further to run on a massively parallel processor (MPP) machine using Message Passing Interface (MPI) routines. All the changes are incorporated using a preprocessor technique such that the same original code works on single and multiple processors as well as on MPP platforms. All the model changes are compared against the single node computation to ensure that the result is bit-by-bit equivalent (assuming that the compiler is the same). The code was designed carefully in such a way that reproducibility of the computation for shared memory and MPP computers was guaranteed in all processor configurations. For the modification of the code to the MPP platforms, two-dimensional decompositions are used for both spectral and grid-point space. This approach made the model flexible to run on any number of processors available. Since climate models tend to run at a relatively low resolution, and the efficiency of the computation on the MPP machines tends to quickly saturate with increasing number of processors, this flexibility is very important for a seasonal prediction model. The model has been tested on multiple platforms ranging from Cray, SGI, SUN, and DEC to Origin 2000, T3E, IBM-SP, and Fujitsu MPP (Juang and Kanamitsu 2001) machines, and has been demonstrated to be very efficient. For example, the T62L28 reduced grid version of the model requires about 20 s of wall-clock time to make a 1-day forecast on an IBM-SP machine using 64 processors. This efficiency makes it possible to conduct a large number of long-term integration experiments and operational runs.

The atmospheric model system is now placed under the Concurrent Versions System (CVS) server. This allows the concurrent development of the model code by multiple developers. The CVS server is accessible from outside NCEP and is released to interested scientists upon request.

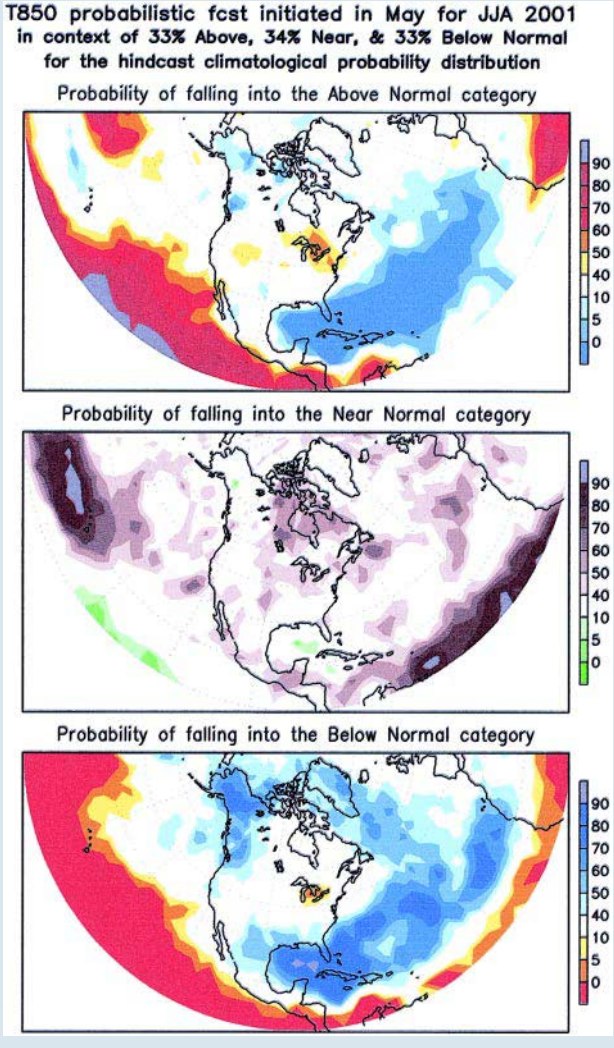

FIG. SB1. An example of the graphical display of a probabilistic 850-hPa temperature forecast for JJA 2001. Initial condition is May 2001. From top to bottom, probability of falling into the above normal, near normal, and below normal categories.

lack of modularity makes it difficult to exchange the package with other land models. This will be improved in the future.

Ocean model. The ocean model is a Pacific basin ocean general circulation model (GCM) that covers the domain 45°S–55°N and 120°E–70°W. This model was originally developed by Bryan (1969) and Cox (1984) and subsequently modified by Philander et al. (1987). The horizontal resolution of the model is 1.5° in the zonal direction and 1/3° in the meridional direction between 10°S and 10°N, linearly increasing to 1° between 10° and 20°, and 1° poleward of 20°N and 20°S. The model has 28 layers in the vertical. This has been our standard configuration since the early 1990s. Further details of the ocean model configuration can be found in Ji et al. (1995). The model is coded to run on shared memory (symmetric multiprocessing) parallel computing architecture. This ocean model is coupled to a T42, 18-level version of the atmospheric model similar to that described earlier. The oceanic and atmospheric models are "one-way anomaly coupled": the total SST from the ocean is given to the atmosphere whereas the anomalies of momentum, heat, and freshwater fluxes from the atmosphere are used to force the ocean model. Further details of the coupled model can be found in Ji et al. (1998).

INITIAL CONDITION. *Atmospheric.* Seasonal prediction has been considered as a boundary forcing problem rather than an initial value problem, and therefore, atmospheric initial conditions have been largely ignored. Most seasonal predictions use long-term simulations, such as Atmospheric Model Intercomparison Project (AMIP) runs, where observed SSTs are given as a boundary condition. The initial condition of the forecast is taken from the end of the simulation. This method has the advantage of eliminating the initial adjustment for the atmosphere but the initial conditions have no relation to the observed atmospheric state.

In the new seasonal prediction system, real-time T62L28 atmospheric analysis from the operational global data assimilation (Kanamitsu 1989) is utilized, in contrast to running in the AMIP mode as in the previous system. Although there is no concrete evidence that the atmospheric initial condition has any impact on seasonal prediction, such a possibility does exist. Atmospheric initial conditions contain both high-frequency and low-frequency components. Examples of low-frequency modes include the PNA and components of North Atlantic oscillation (NAO) and Arctic Oscillation (AO) modes. If the model can predict (or maintain) these low-frequency modes, atmospheric initial conditions may be of some importance. But these initial conditions may lack impact due to large systematic errors, which distort the low-frequency part of the atmospheric variability during the early part of the integration.

There is an additional reason for using atmospheric analysis as an initial condition. At NCEP, numerical predictions for different lead times (short range, medium range, week-2, month, and season) are produced by several different model systems and accordingly these forecasts suffer from discontinuities. Using the same model and the same initial condition for short to seasonal range prediction would eventually eliminate this discontinuity, and instead create a "seamless" suite of products. The use of atmospheric analysis for the initial condition of seasonal prediction is one step toward this goal.

Land surface. While the importance of soil wetness to summer and spring predictability is recognized, lack of observations in most regions makes it difficult to incorporate soil moisture into the operational forecasts. The same applies to snow depth. The water equivalent snow depth is a major factor in soil wetness during spring through snow melt. Again, observations are scarce with the exception of snow cover, which cannot be easily converted to snow depth.

Currently, the best soil wetness and snow depth "analyses" are derived from a land hydrology model with modeled or observed precipitation and surface energy fluxes. This is the Land Data Assimilation System (LDAS; Mitchell et al. 2000), which is similar to atmospheric data assimilation, but without insertion of observed soil parameters. Therefore, the product is strongly dependent on the accuracy of the hydrology model. The method, however, has an advantage of providing model-consistent land conditions, because the same hydrology model is used to obtain the initial condition and eliminating the initial adjustment problem in the land hydrology (which may have very long timescales of months to years). Since the global soil wetness observations are extremely sparse, this is the best method available at present. The adoption of this method implies that the seasonal prediction system requires its own data assimilation for land surface initial conditions, just like the medium-range prediction system requires its own atmospheric data assimilation as an essential part of the prediction system.

In Reanalysis-2, observed pentad precipitation forced the land hydrology model, similar to the LDAS procedure. The resulting soil wetness analysis was far

superior to those used in Reanalysis-1. Since the seasonal prediction model is similar to the Reanalysis-2 model, this soil wetness analysis is ideal for land surface initial conditions in the NCEP seasonal forecast system (at least for forecast runs in the 1979–99 period when the Reanalysis-2 product is available).

In the new seasonal prediction system, climatological soil wetness and snow from the Reanalysis-2 is used initially, since the real-time global soil wetness analysis is not yet available. We are hoping to extend the Reanalysis-2 to real time for obtaining these initial conditions sometime in 2002. From Fig. 5, it is apparent that the use of the Reanalysis-2 soil wetness condition significantly improves the 1-month lead 2-month-averaged 2-m temperature prediction.

Vegetation cover and types are other factors that can provide forcing over land. Although these parameters do not vary significantly from one year to the next, they vary appreciably on timescales of decades. Since the hindcasts over the 1979–99 period are an essential part of the seasonal prediction, as will be discussed later, the change in these parameters must be accurately incorporated into the system. However, due to the lack of observed historical vegetation cover, a climatological distribution is currently used in all of our integrations.

Oceanic. The initial conditions for the ocean are obtained from an ocean data assimilation system that was originally developed at NOAA's Geophysical Fluid Dynamics Laboratory. The ocean data assimilation system uses a three-dimensional variational scheme developed by Derber and Rosati (1989). This system was implemented at NCEP in the early 1990s (Ji et al. 1995) and subsequently improved to include assimilation of sea surface height observations as well as temperature observations (Behringer et al. 1998). The present system assimilates real-time, in situ subsurface ocean temperature observations collected from NOAA's operational ENSO observing system, and SST and sea surface height variations observed from satellites. The ocean data assimilation system is running in real time once each week to produce weekly ocean analyses and initial conditions for the coupled forecast model.

Ensemble forecasts. Because it is inherently probabilistic, seasonal prediction must use an ensemble method. However, the rationale for ensemble prediction is different for short-to-medium-range prediction than for seasonal predictions. In the former, ensemble average helps sample the uncertainty in the initial condition. In the latter, the ensemble prediction samples the range of outcomes of the seasonal mean atmospheric state.

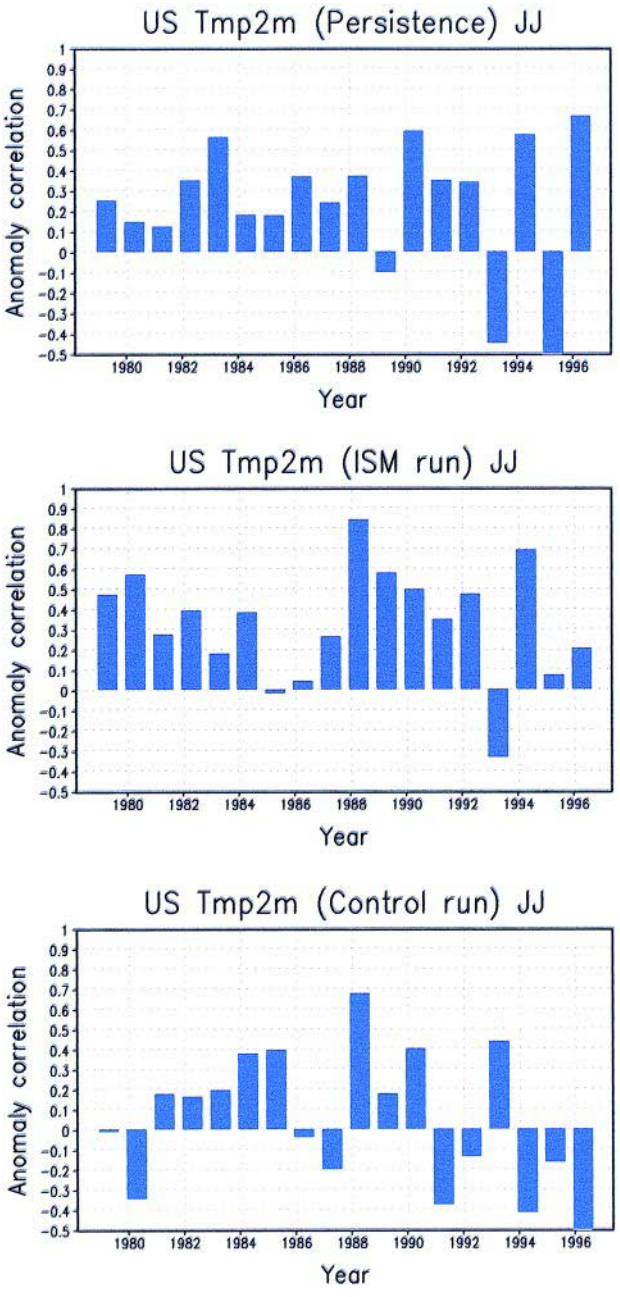

Fig. 5. An example of the impact of soil wetness initial conditions. Comparisons of the near-surface air temperature skill scores (%) from 10-member ensemble 18-yr (1979–96) hindcasts for runs with climatological land conditions and with runs with the Reanalysis-2 soil wetness initial conditions. For reference, the anomaly persistence forecast is also presented: (top) anomaly persistence, (middle) forecast with analysis soil wetness initial condition, and (bottom) forecast with climatological soil wetness initial condition.

The requirement for the number of ensemble members has been debated by many (e.g., Kumar and

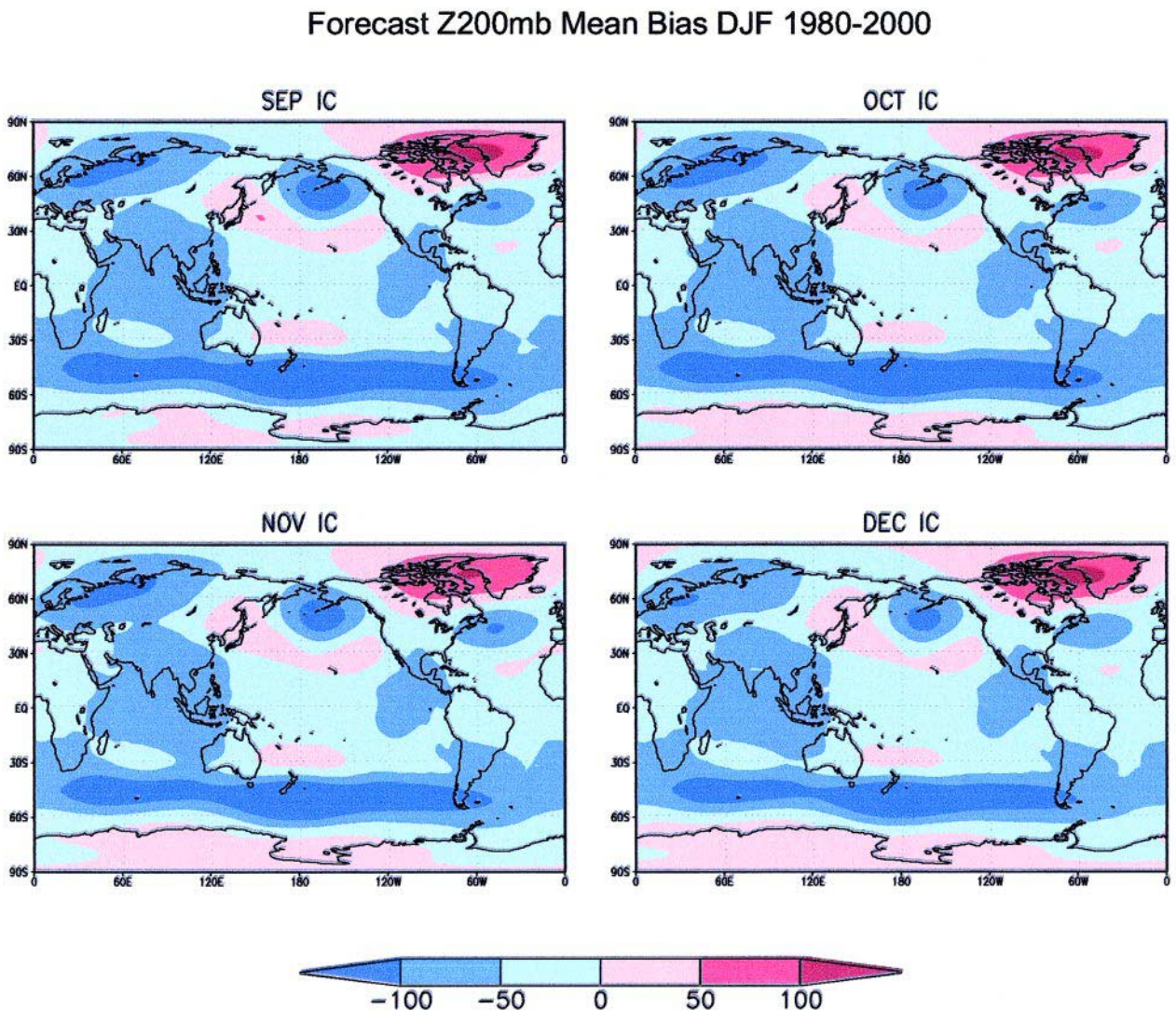

Fig. 6. 200-hPa height systematic error (m) for JFM computed from 1980–2000 hindcasts. (top left) Sep initial conditions, (top right) Oct initial conditions, (bottom left) Nov initial conditions, and (bottom right) Dec initial conditions. Note that the systematic error is not strongly dependent on the forecast lead time.

Hoerling 2000), and the ensemble size is believed to depend on the magnitude of the external forcing. An order of 10 or more is considered to be reasonable for the estimate of the first moment, and some second moments (Kumar et al. 2000), which increases dramatically for the correct estimates of second and higher moments (Sardeshmukh et al. 2000). The number is practically limited by available computer resources. In the new system, we have chosen 20 members for the forecast. The corresponding initial conditions are chosen from 5 days prior and after the beginning of the month at 12-h intervals.

Since ensemble averaging removes seasonal mean atmospheric noise, the amplitude of the ensemble mean anomaly forecast tends to be less than the observed amplitude. It is important to recognize this difference in amplitude when the ensemble mean is used for seasonal forecasting.

Systematic error correction. There is one practical but important procedure left to describe in the seasonal prediction system: the systematic error or bias of the model. The systematic error of the numerical model is of the same magnitude as a moderate anomaly (up to 100 m for 200-hPa height) as shown in Fig. 6, and it degrades the model forecast enough to make the direct model output very difficult to use. In order to correct this error, a standard procedure is to calculate anomalies from "model climatology" instead of from observed climatology. This procedure is equivalent to making a systematic error correction to the model prediction, because the difference between the

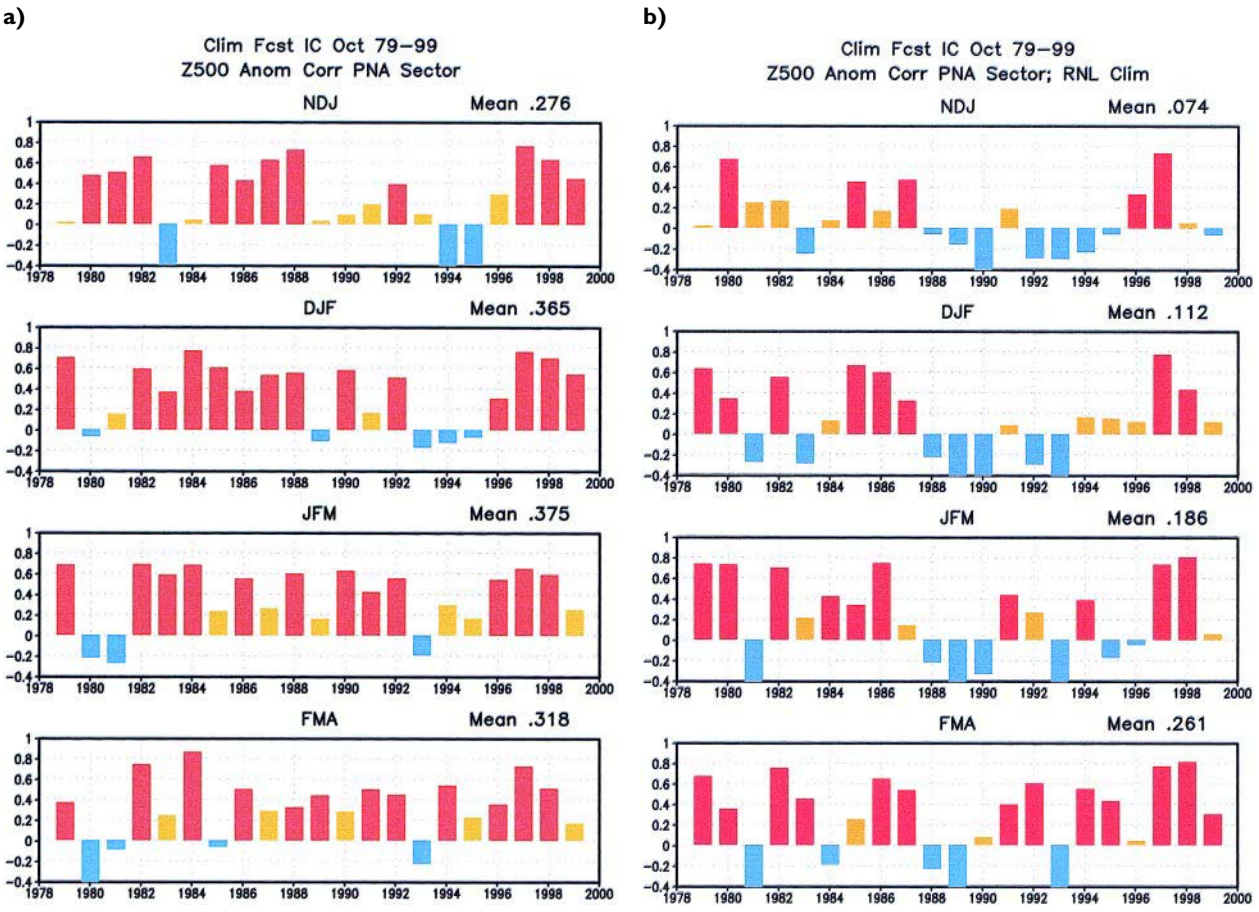

FIG. 7. Effect of the use of a different climatology for the anomaly correlation calculation: (a) anomaly correlation of 500-hPa height over the PNA region using Reanalysis-1 as a climatology, and (b) using average of 21-yr 10-member ensemble forecasts as a climatology. The correlation for each year is computed from the mean of the 10-member ensemble forecast.

model climatology and the observed climatology (which is the systematic error of the model) is subtracted from the model forecast. This process significantly increases the forecast skill of the model. An example of the effect of systematic error correction is presented in Figs. 7a and 7b, where the anomaly correlation scores of 500 hPa are compared for NDJ, DJF, JFM, and FMA periods over North American region for the last 21 yr. The systematic error correction improves the 21-yr average scores from 0.074 to 0.276, 0.112 to 0.365, 0.186 to 0.375, and 0.261 to 0.318 for the four 3-month means. The systematic error of the model is easily calculated as a long-term mean from the simulation if the forecast is running in an AMIP mode. In the forecast mode with analyzed atmospheric initial conditions, it is more problematic because the model atmosphere goes through initial adjustment processes and the systematic error becomes a function of forecast lead time (as well as of the initial month). The best method to obtain model climatology is to make a large number of past case predictions (i.e., hindcasts).

In both situations, the most serious problem of using model climatology is that it places severe restrictions on the model updates. This is because every time the model physics and/or initial surface conditions change, the systematic error changes as well, and the model climatology must be recalculated. The computation of model climatology requires large amounts of computer resources, restricting frequent changes to the model. To the model developer, this is a very serious practical restriction. A similar struggle developed between modeler and model user several decades ago for short-range predictions, when the use of model output statistics (MOS) prevented frequent changes to the forecast model.

In the new system, we decided to include hindcasts in the operational real-time forecast. Ensemble hindcasts for the same month from the last 21 yr are made before the real-time forecasts start, so that the

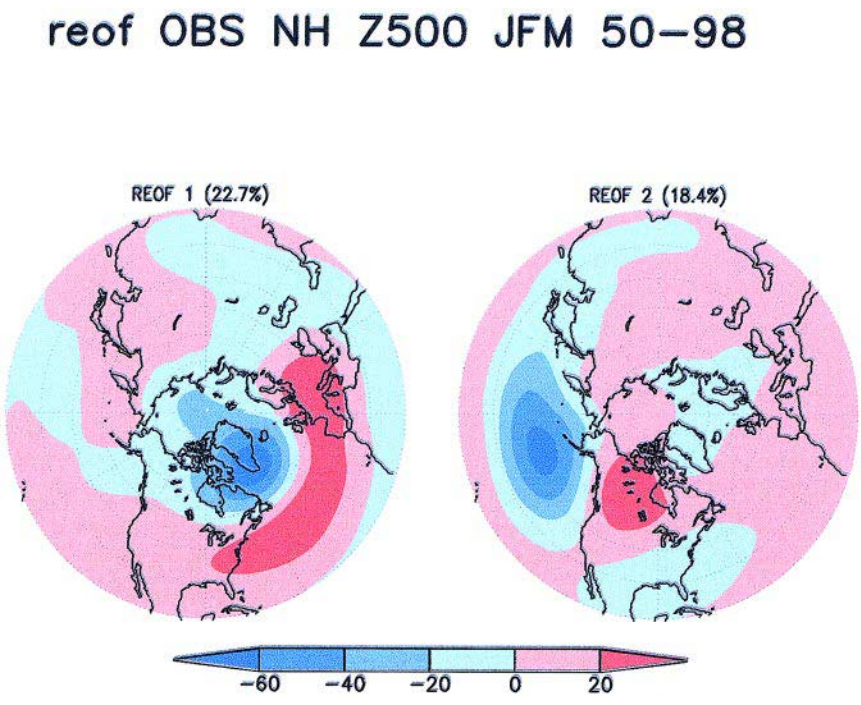

Fig. 8. Observed NAO and PNA modes (m) used to obtain Fig. 9. Modes are computed from 1950–99 Reanalysis-1.

model climatology for that month is ready. Since real-time forecasts are done once a month, there is ample time to make the hindcasts prior to the real-time forecasts. This procedure allows the model to be updated when needed, thus providing flexibility to the model developers. The model has already been updated twice since April 2000, to reduce the systematic warm bias and to fix other errors. The shortcoming of this approach is that the model may not remain fixed long enough to yield performance over an annual cycle. However, this should not cause any practical problems for monthly operational forecasts.

In the current setting, we use 10-member ensembles (instead of 20 in the real-time forecast) in the hindcasts, starting at 0000 and 1200 UTC of days 1–5 of each month. The hindcasts use observed SSTs during the integration, which provides the upper limit of the model skill. The initial conditions of soil wetness and snow are climatology from the Reanalysis-2 for both hindcasts and forecasts since real-time analysis of these fields are not available for forecast yet. This procedure assures that the hindcast climatology is consistent with the forecast. The system does not include vegetation variations, and sea ice cover is climatology.

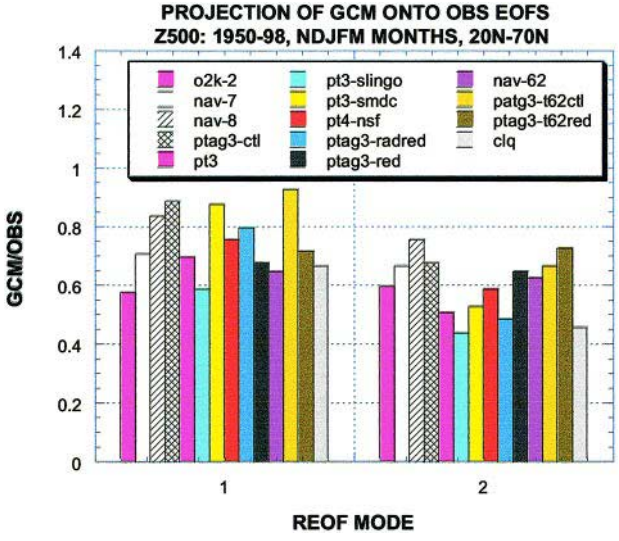

Fig. 9. Ratios of the amplitude of NAO and PNA modes between simulated and observed 500-hPa height for various experiments from 50-yr AMIP runs. EOF mode 1 and 2 are shown in Fig. 8 and correspond to NAO and PNA modes, respectively. Each bar denotes different experiment. The detail of each experiment is not relevant to the paper and is not explained.

The hindcasts are also important in providing model performance history. They can be used to create geographically varying "skill masks" based on the global coverage of the temporal skill. They can also be used to create a type of "composite skill mask" to find the model skill for particular conditions, such as warm or cold ENSO events. Currently, NCEP's Climate Prediction Center (CPC) combines dynamical and statistical prediction methods with their own skill masks as weighting factors to make the official monthly and seasonal long-lead outlooks.

MODEL PERFORMANCE. *Interannual variability in the AMIP runs.* With the changes to the Reanalysis-2 version of the atmospheric model based on idealized ENSO experiments, the model needs to be further tested in more realistic conditions. For this purpose, several 50-yr AMIP runs were made with various model configurations. The detailed responses of the models were examined in two ways: one to look

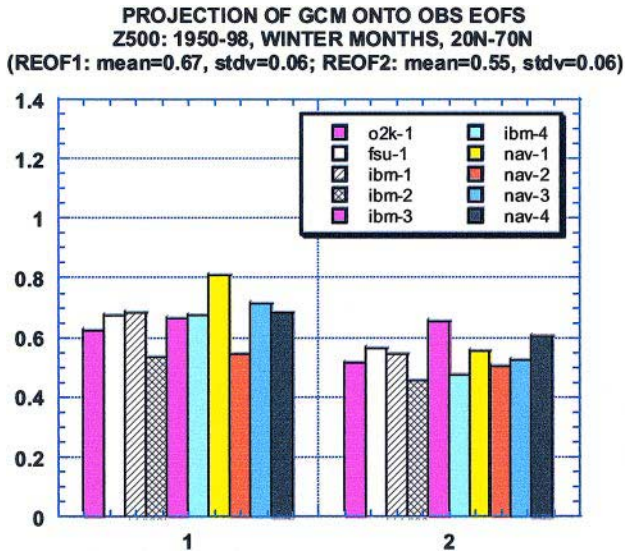

FIG. 10. Same as in Fig. 9 but computed from 10-member 50-yr ensemble AMIP runs made on various machines and slightly perturbed initial conditions. Each bar corresponds to each ensemble member. O2k stands for the run made on the CMP Origin 2000 machine, FSU stands for the run made at Florida State University's COAPS using their Origin 2000 machine, ibm stands for the runs made on NCEP's IBM-SP machine, and nav stands for the runs made on the U.S. Navy's origin 2000 machine.

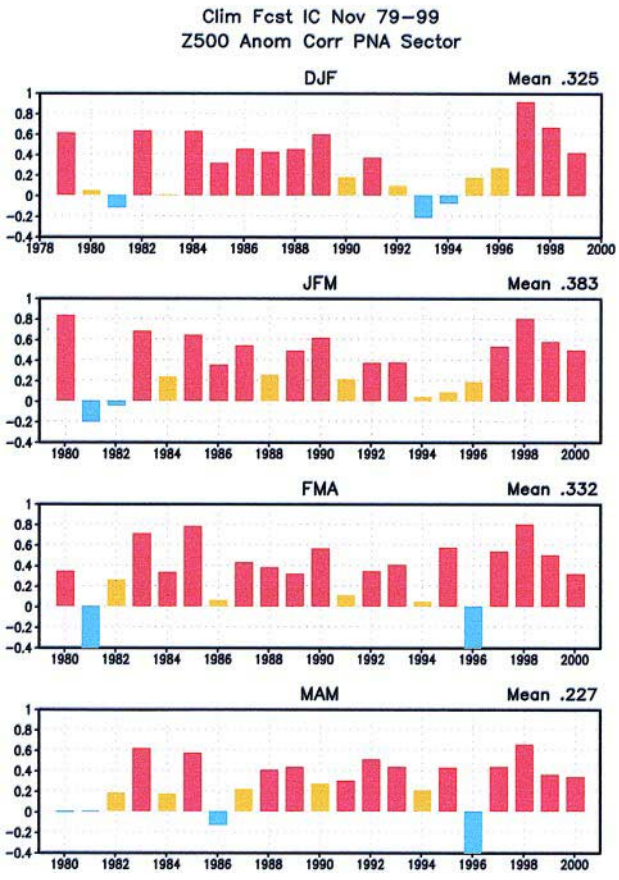

FIG. 11. Anomaly correlation of 3-month average 10-member ensemble mean 500-hPa height hindcasts for DFJ, JFM, FMA, and MAM over the PNA sector. Initial conditions are November of each year. Each bar is computed from a 10-member ensemble mean.

at the strong warm and cold ENSO composites and to compare them to the observations, and the other to examine the atmospheric low-frequency variability. The former evaluation was subjective and the results are not shown here. In the latter, we projected the model-simulated interannual variability onto the leading modes of observed interannual variability (mainly NAO mode and PNA mode; Fig. 8) for various model configurations and assessing their projection amplitude. Figure 9 shows the ratio of the amplitude of the modes for various experiments from 50-yr AMIP runs. Modes 1 and 2 correspond to the NAO and PNA modes, respectively. The purpose of the figure is to present the variability of this ratio from experiment to experiment, and detailed description of each experiment is intentionally avoided. The variation in the projected amplitude among experiments is considerable and some model configurations are apparently better than others. One point to note is the stability of these computations. We examined this by using the 10-member ensemble 50-yr AMIP runs all performed with exactly the same model. Figure 10 shows the variability of the scores among the ensemble members. It indicates that the variability can be as large as the variations between the different model experiments. Therefore, the skill comparison from one 50-yr simulation does not represent overall model performance. For this reason, this verification method was only used as a guidance in testing whether a particular version of the model performs significantly worse than others.

Hindcast performance. The performance of the atmospheric model is better represented by examining the skill of the hindcasts forced with observed SSTs. Figure 11 shows 10-member ensemble hindcast anomaly correlations of the 500-hPa height over the PNA region during the winter–spring season. These hindcasts were started from the first 5 days of November, 12 h apart, for the period 1979–99, and four lead times of 1–4 months, corresponding to DJF, JFM, FMA, and MAM forecasts are presented. The 21-yr mean anomaly correlation is highest in JFM (0.383). The score for some individual years exceeds 0.8. Note that these scores are comparable to those of other seasonal prediction models (Shukla et al. 2000; Kang et

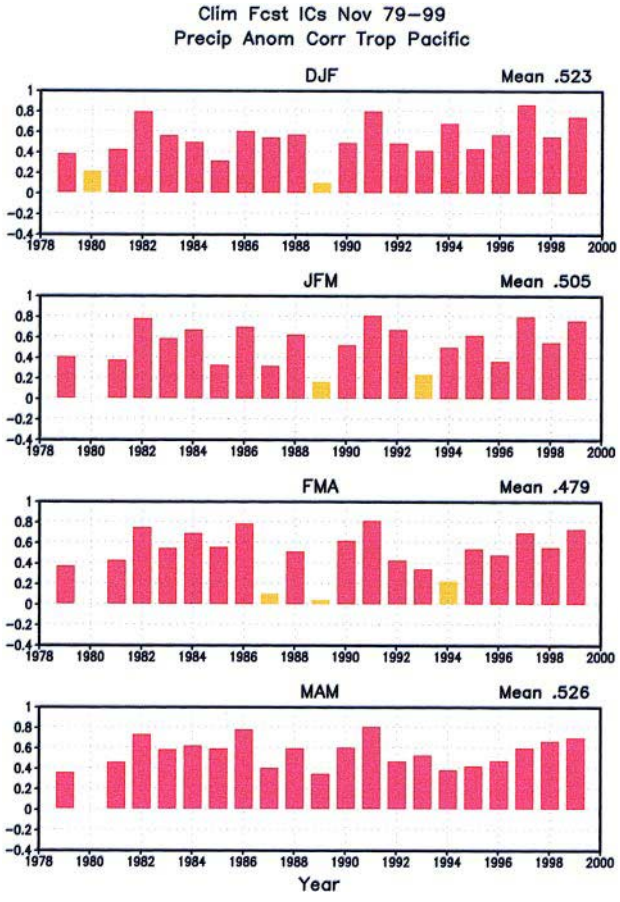

Fig. 12. Anomaly correlation of precipitation hindcasts over the tropical Pacific. The month of initial state is Nov and scores for average DJF, JFM, FMA, and MAM are shown. The correlation for each year is computed from the mean of a 10-member ensemble forecast. The 21-yr average correlation is shown at the upper right of each figure.

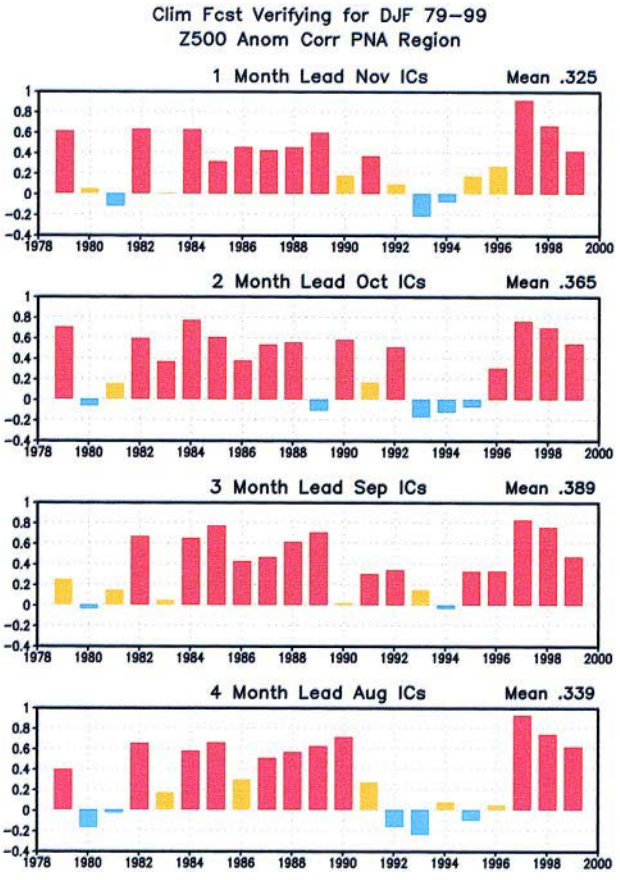

Fig. 13. Anomaly correlation of 3-month mean 500-hPa height hindcasts for DJF over the PNA region. Each figure corresponds to the forecast started from a different month. (top) Nov initial condition (1-month lead); (second from top) Oct initial condition (2-month lead); (third from top) Sep initial condition (3-month lead); (bottom) Aug initial condition (4-month lead).

al., personal communication). The skillful hindcasts are due to the good response of the tropical precipitation anomaly to observed SST anomalies over the tropical Pacific (Fig. 12) with the 21-yr mean anomaly correlation ranging from 0.526 to 0.479 and approaching 0.9 in some individual years. As a more strict comparison, we performed the same skill score computations as those performed by Anderson et al. (1999). They compared 700-hPa height forecast skill over North American region between the GFDL and the old version of the NCEP seasonal forecast model. According to the latest comparison, the current seasonal forecast model performs much better than the old version and about the same or slightly better than the GFDL model as shown in Table 2. The improvement in model physics apparently contributed to the increase in the model skill. Looking closely at Fig. 11, the model prediction is better for the years with larger tropical Pacific SST anomalies (see warm events in 1982, 1986, and 1997 and cold events in 1984, 1988, and 1998 initial conditions for DJF forecast), which is reflected in the skill score of the tropical precipitation (Fig. 12). None of the years with low skill scores had a large tropical SST anomaly. But the opposite is not the case, there are years with high skill scores in both the PNA sector (Fig. 11) and the tropical Pacific (Fig. 12) without large SST anomaly (e.g., 1990 for JFM and FMA forecasts). The sources of predictability in these cases are unknown and need further investigation. The skill of the winter season forecasts (DJF) started from different months, but verified for the same season (i.e., forecasts with different lead times), are displayed in Fig. 13. They are generally very similar but with some differences, suggesting that the atmospheric initial condition does not have a significant impact during the summer season, at least for this system.

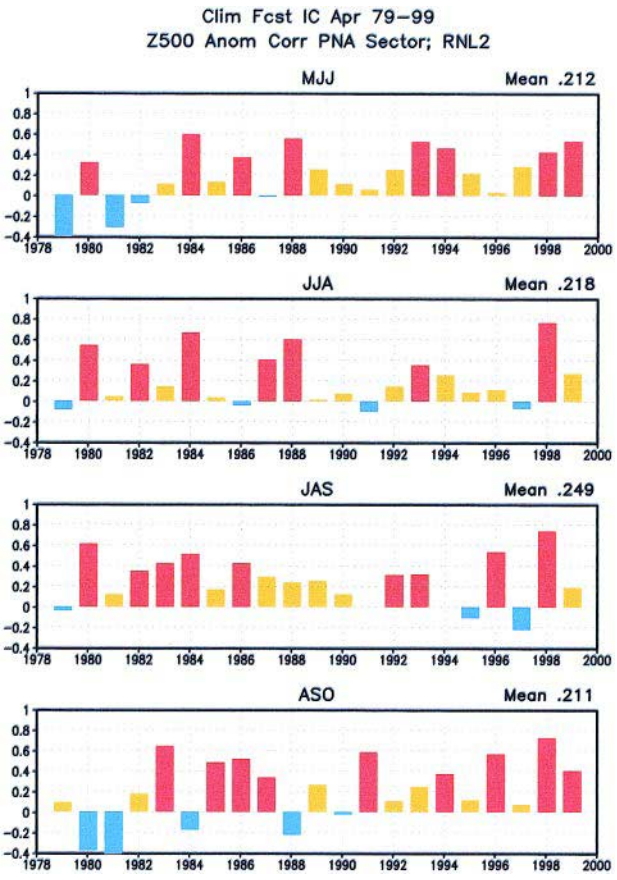

Fig. 14. Anomaly correlation of 3-month average 10-member ensemble mean 500-hPa hindcasts for MJJ, JJA, JAS, and ASO. Verification is against Reanalysis-2. Initial conditions are Apr.

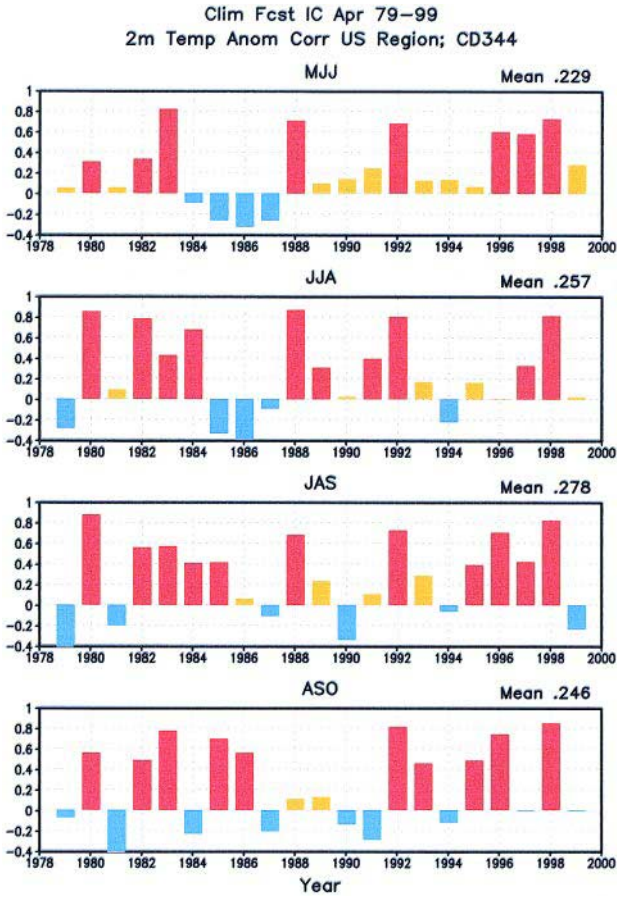

Fig. 15. Same as in Fig. 14 but for 2-m temperature. Verification is against independent Climate Division 344 data.

During summer, the geopotential height forecast is generally much worse (mean 0.211–0.249, with maximum of 0.6–07 as shown in Fig. 14). However, we found that there is higher skill in predicting near surface temperature over land (mean 0.229–0.278, with maximum reaching 0.9) as shown in Fig. 15. Since the only external forcing in these hindcasts is the SST anomaly, this predictability most likely came from SST anomalies. The use of Reanalysis-2 "observed" soil wetness in the initial state will further increase the model skill as shown in Fig. 5.

The model skill score of the real-time operational forecast is displayed in Fig. 16. Since the forecast skill strongly depends on magnitude of the tropical SST anomalies as shown earlier, the comparison of skill among forecasts made before and after April 2000 does not provide valid information on how the two different models performed. The new model is showing usable skill for near-surface temperature and precipitation (except July, August, and September) despite the fact that SST forcing is very weak. However, this weak forcing is reflected in the poor prediction of 200-hPa height. The skill of near-surface temperature is probably coming from the sea surface temperature at the beginning of the prediction, which creates anomalies in the soil wetness that in turn influence the surface temperature prediction. These processes need to be verified in future work. The failure of pre-

Table 2. Comparison of 700-mb forecast anomaly correlation for JFM over the PNA region, averaged over years 1980–88. SFM is the new version of the seasonal forecast model, B9X is the old version, and GFDL is the GFDL model.

	JFM	FMA	MAM
SFM	0.40	0.42	0.34
B9X	0.30	0.35	0.32
GFDL	0.35	0.42	0.36

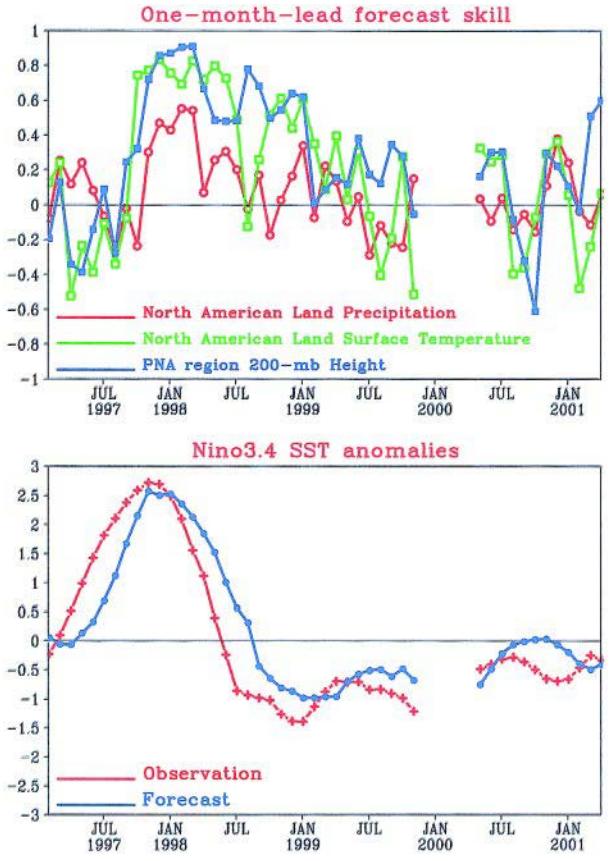

Fig. 16. One-month lead 3-month average operational seasonal forecast anomaly correlation scores of North American land precipitation (red), North American land surface temperature (green), and 200-hPa height over the PNA region (blue) for the period 1997–2001 shown in the top panel. The period where the lines are missing is when the dynamical model was not run due to a computer fire, and the model is the old version prior to this period. The observed (blue) and predicted (red) SST anomaly in the Niño-3.4 area is also shown in the bottom panel.

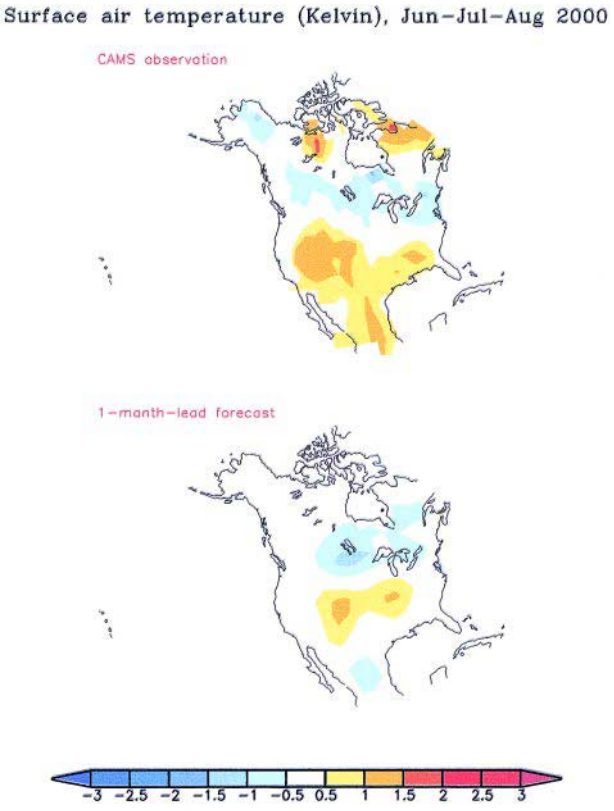

Fig. 17. An example of excellent near-surface temperature anomaly forecast (K). The 20-member ensemble average 2-m temperature prediction for JJA 2000: (top) observation; (bottom) forecast. Initial condition is May.

diction during July–August–September is likely due to the lack of initial soil wetness anomalies in these runs.

Finally, we will show an example of an excellent real time forecast together with the verifying map of near surface temperature over North America during JJA of 2000 in Fig 17. The warm anomaly in the middle of the United States and the cold anomaly in Canada were well predicted by the model. Note that the magnitude of the predicted anomaly is less than observed due to the ensemble averaging discussed earlier in the paper.

Plans for improvements. The atmospheric model resolution was increased from T42L28 to reduced grid T62L28 in April 2001. The high-resolution model performs better at the large scale as well as in near-surface temperature prediction and simulation of transient activities. This higher-resolution model can also provide useful forecasts of tropical disturbances, which will be reported in the future. The atmospheric portion of the seasonal prediction model was recently placed into the official operational suite of the NCEP Central Operations. This freed our staff from the intense monitoring work and allowed us to concentrate more on the application of the product. The seasonal prediction system was different than the daily short- and medium-range predictions and this work was a big challenge.

The use of Reanalysis-2 soil wetness initial conditions will be performed by the spring of 2003. The extension of the Reanalysis-2 to near–real time to produce soil wetness and snow depth analyses is in progress. In the near future, the physics of the atmospheric model will be upgraded to include liquid water prediction, more physically realistic cloud schemes, and Kim and Arakawa (1995) gravity wave

PRODUCTS

Monthly average of all the members from forecast and hindcasts, as well as daily output of selected variables, are archived for future research. The past 2–3 months of ensemble average of forecasts, hindcasts, and model climatology are available online at a public NCEP ftp site (ftp://tgftp.nws.noaa.gov/SL.us008001/ST.opnl/MT.clim_MR.hind/ and ftp://tgftp.nws.noaa.gov/SL.us008001/ST.opnl/MT.clim_MR.fcst).

The graphical output of near surface temperature, precipitation, and 200-hPa height anomalies over the globe and over the continental United States are available online at the NCEP Web site (www.emc.ncep.noaa.gov/research/cmb/atm_forecast/images and www.cpc.ncep.noaa.gov/schemm).

These sites also display past performance of the model. The latest products are available on the ftp server by the 10th of each month. In addition to these standard products, CPC produces supplemental outputs such as hindcast skill spread chart, monthly variance of daily fields, and anomaly probability maps. An example of the anomaly probability map forecast is shown in Fig. SB1.

drag. The ocean model and the ocean assimilation system will be updated to a global domain. The two-tier approach will continue, but more work toward a one-tier system will be emphasized. The coupling with the sea ice model will also be accelerated. Additional experimental 4-month forecasts will be performed using persistent anomaly SSTs in collaboration with Recherche en Prévision Numérique (RPN) and the Canadian Center for Climate Modeling and Analysis as part of their Historical Forecast Project (Derome et al. 2000, manuscript submitted to *Atmos.–Ocean*). This is an alternative (and inexpensive) approach to extended-range prediction without an ocean model.

ACKNOWLEDGMENTS. We would like to give our sincere thanks to Dr. Ants Leetmaa, who strongly pushed this project to success. We thank Prof. J. O'Brien of the Center for Ocean–Atmospheric Prediction Studies (COAPS), The Florida State University for kindly supplying computer time to make one of the AMIP runs. Thanks are also due to Dr. Wayne Higgins and Dr. Tom Fahey, whose review significantly improved the manuscript, and to Jeff Rosenfeld who helped in improving the manuscript.

APPENDIX: SUMMARY OF ACRONYMS USED IN THIS PAPER.

AMIP	Atmospheric Model Intercomparison Project
AO	Arctic Oscillation
ASO	August–September–October
CCM	Community Climate Model
CMP	coupled modeling project
COAPS	Center for Ocean–Atmospheric Prediction Studies
CPC	Climate Prediction Center
CVS	Concurrent Versions System
DJF	December–January–February
DOE	Department of Energy
ENSO	El Niño–Southern Oscillation
FMA	February–March–April
GCM	general circulation model
GFDL	Geophysical Fluid Dynamical Laboratory
GSFC	Goddard Space Flight Center
JAS	July–August–September
JFM	January–February–March
JJA	June–July–August
LDAS	Land Data Assimilation System
MAM	March–April–May
MJJ	May–June–July
MOS	model output statistics
MPI	Message Passing Interface
MPP	massively parallel processing
MRF	Medium Range Forecast model
NAO	North Atlantic Oscillation
NCAR	National Center for Atmospheric Research
NCEP	National Centers for Environmental Prediction
NDJ	November–December–January
NOAA	National Oceanic and Atmospheric Administration
OSU	Oregon State University
PNA	Pacific–North American teleconnection
RAS	Relaxed Arakawa–Schubert parameterization
RNL	Reanalysis (NCEP–NCAR reanalysis)
RNL2	Reanalysis-2 (NCEP–DOE reanalysis)
RPN	Recherche en Prévision Numérique
SAS	Simplified Arakawa–Schubert parameterization
SST	sea surface temperature
SSTA	sea surface temperature anomaly

REFERENCES

Alpert, J. C., M. Kanamitsu, P. M. Caplan, J. G. Sela, G. H. White, and E. Kalnay, 1988: Mountain induced

gravity wave drag parameterization in the NMC medium-range model. Preprints, *Eighth Conf. on Numerical Weather Prediction,* Baltimore, MD, Amer. Meteor. Soc., 726–733.

Anderson, J., H. Van den Dool, A. Barnston, W. Chen, W. Stern, and J. Ploshay, 1999: Present-day capabilities of numerical and statistical models for atmospheric extratropical seasonal simulation and prediction. *Bull. Amer. Meteor. Soc.,* **80,** 1349–1362.

Behringer, D., M. Ji, and A. Leetmaa, 1998: An improved coupled model for ENSO prediction and implications for ocean initialization. Part I: The ocean data assimilation system. *Mon. Wea. Rev.,* **126,** 1013–1021.

Bryan, K., 1969: A numerical model for the study of the World Ocean. *J. Comput. Phys.,* **4,** 347–376.

Chen, F., and Coauthors, 1996: Modeling of land surface evaporation by four schemes and comparison with FIFE observations. *J. Geophys. Res.,* **101,** 7251–7268.

Chou, M.-D., 1992: A solar radiation model for use in climate studies. *J. Atmos. Sci.,* **49,** 762–772.

——, and M. J. Suarez, 1994: An efficient thermal infrared radiation parameterization for use in general circulation models. NASA Tech. Rep. TM-1994-104606 Series on Global Modeling and Data Assimilation, 85 pp.

——, and K.-T. Lee, 1996: Parameterizations for the absorption of solar radiation by water vapor and ozone. *J. Atmos. Sci.,* **53,** 1203–1208.

Cox, M. D., 1984: A primitive, 3-dimensional model of the ocean. GFDL Ocean Group Tech. Rep. 1, 143 pp.

Derber, J., and A. Rosati, 1989: A global oceanic data assimilation system. *J. Phys. Oceanogr.,* **19,** 1333–1347.

Derome, J., and Coauthors, 2000: Seasonal predictions based on two dynamical models. *Atmos.–Ocean,* submitted.

Dorman, J. L., and P. J. Sellers, 1989: A global climatology of albedo, roughness and stomatal resistance for atmospheric general circulation models as represented by the Simple Biosphere Model (SB). *J. Appl. Meteor.,* **28,** 833–855.

Fels, S. B., and M. D. Schwarzkopf, 1975: The simplified exchange approximation: A new method for radiative transfer calculations. *J. Atmos. Sci.,* **32,** 1475–1488.

Garrat, J. R., 1993: Sensitivity of climate simulations to land-surface and atmospheric boundary-layer treatments—A review. *J. Climate,* **6,** 419–449.

Hong, S.-Y., and H.-L. Pan, 1996: Nonlocal boundary layer vertical diffusion in a medium-range forecast model. *Mon. Wea. Rev.,* **124,** 2322–2339.

Jarraud M., A. J. Simmons, and M. Kanamitsu, 1988: Sensitivity of medium-range weather forecasts to the use of an envelope orography. *Quart. J. Roy. Meteor. Soc.,* **114,** 989–1025.

Ji, M., A. Leetmaa, and J. Derber, 1995: An ocean analysis system for seasonal to interannual climate studies. *Mon. Wea. Rev.,* **123,** 460–481.

——, D. W. Behringer, and A. Leetmaa, 1998: An improved coupled model for ENSO prediction and implications for ocean initialization. Part II: The coupled model. *Mon. Wea. Rev.,* **126,** 1022–1034.

Juang, H.-M. H., and M. Kanamitsu, 2001: The computational performance of the NCEP Seasonal forecast model on Fujitsu VPP5000 at ECMWF. *Proc. Ninth ECMWF Workshop on the Use of High Performance Computing in Meteorology,* Shinfield Park, Reading, United Kingdom, ECMWF.

Kalnay, E., and Coauthors, 1996: The NCEP/NCAR 40-Year Reanalysis Project. *Bull. Amer. Meteor. Soc.,* **77,** 437–471.

Kanamitsu, M., 1989: Description of the NMC Global Data Assimilation and Forecast System. *Wea. Forecasting,* **4,** 335–342.

——, W. Ebisuzaki, J. Woollen, S.-K. Yang, J. Hnilo, M. Fiorino, and J. Potter, 2001: NCEP/DOE AMIP-II Reanalysis (R-2). *Bull. Amer. Meteor. Soc.,* in press.

Kim, Y.-J., and A. Arakawa, 1995: Improvement of orographic gravity wave parameterization using a mesoscale gravity wave model. *J. Atmos. Sci.,* **52,** 1875–1902.

Koster, R. D., M. J. Suarez, and M. Heiser, 2000: Variance and predictability of precipitation at seasonal-to-interannual timescales. *J. Hydrometeor.,* **1,** 26–46.

Kumar, A., and M. P. Hoerling, 2000: Analysis of a conceptual model of seasonal climate variability and implications for seasonal prediction. *Bull. Amer. Meteor. Soc.,* **81,** 255–264.

——, ——, M. Ji, A. Leetmaa, and P. Sardeshmukh, 1996: Assessing a GCM's suitability for making seasonal predictions. *J. Climate,* **9,** 115–129.

——, A. Barnston, P. Peng, M. Hoerling, and L. Goddard, 2000: Changes in the spread of the variability of the seasonal mean atmospheric states associated with ENSO. *J. Climatol.,* **13,** 3139–3151.

Kuo, H. L., 1965: On the formation and intensification of tropical cyclones through latent heat release by cumulus connection. *J. Atmos. Sci.,* **22,** 40–63.

Lacis, A. A., and J. E. Hansen, 1974: A parameterization for the absorption of solar radiation in the Earth's atmosphere. *J. Atmos. Sci.,* **31,** 118–133.

Mitchell, K., and Coauthors, 2000: The collaborative GCIP land data assimilation (LDAS) project and supportive NCEP uncoupled land-surface modeling initiatives. Preprints, *15th Conf. on Hydrology,* Long Beach, CA, Amer. Meteor. Soc., 1–4.

Miyakoda, K., and J. Sirutis, 1986: Manual of the E-physics. 67 pp. [Available from GFDL, Princeton University, P.O. Box 308, princeton, NJ 08542.]

Moorthi, S., and M. J. Suarez, 1992: Relaxed Arakawa–Schubert: A parameterization of moist convection for general circulation models. *Mon. Wea. Rev.,* **120,** 978–1002.

——, and ——, 1999: Documentation of version 2 of relaxed Arakawa–Schubert cumulus parameterization with convective downdrafts. NOAA Tech. Rep. NWS/NCEP 99-01, U.S. Department of Commerce, 44 pp.

Pan, H.-L., and L. Mahrt, 1987: Interaction between soil hydrology and boundary layer developments. *Bound.-Layer Meteor.,* **38,** 185–202.

——, and W.-S. Wu, 1995: Implementing a mass flux convection parameterization package for the NMC Medium-Range Forecast Model. NMC Office Note 409, 40 pp. [Available from NCEP/EMC 5200 Auth Road, Camp Springs, MD 20746.]

Philander, S. G., W. J. Hurlin, and A. D. Seigel, 1987: A model of the seasonal cycle in the tropical Pacific ocean. *J. Phys. Oceanogr.,* **17,** 1986–2002.

Reynolds, R. W., and T. M. Smith, 1994: Improved global sea surface temperature analyses using optimum interpolation. *J. Climate,* **7,** 929–948.

Roads, J. O., S-C. Chen, and F. Fujioka, 2001: ECPC's weekly to seasonal global forecasts. *Bull. Amer. Meteor. Soc.,* **82,** 639–658.

Sardeshmukh, P. D., G. O. Compo, and C. Penland, 2000: Changes of probability associated with El Niño. *J. Climate,* **13,** 4268–4286.

Schwarzkopf, M. D., and S. B. Fels, 1985: Improvements to the algorithm for computing CO2 transmissivities and cooling rates. *J. Geophys. Res.,* **90,** 10 541–10 550.

——, and ——, 1991: The simplified exchange method revisited: An accurate, rapid method for computation of infrared cooling rates and fluxes. *J. Geophys. Res.,* **96,** 9075–9096.

Shukla, J., and Coauthors, 2000: Dynamical seasonal prediction. *Bull. Amer. Meteor. Soc.,* **81,** 2593–2606.

Slingo, J. M., 1987: The development and verification of a cloud prediction model for the ECMWF model. *Quart. J. Roy. Meteor. Soc.,* **113,** 899–927.

Tiedtke, M., 1983: The sensitivity of the time-mean large-scale flow to cumulus convection in the ECMWF model. *Proc. ECMWF Workshop on Convection in Large-Scale Models,* Reading, England, ECMWF, 297–316.

Williamson, D., and J. Rosinski, 2000: Accuracy of reduced-grid calculations. *Quart. J. Roy. Meteor. Soc.,* **126,** 1619–1640.

Zhang, G. J., and N. A. Mcfarlane, 1995: Sensitivity of climate simulations to the parameterization of cumulus convection in the Canadian Climate Centre general circulation model. *Atmos.–Ocean,* **33,** 407–446.